Am J Physiol Heart Circ Physiol 316: H1005–H1013, 2019.
First published March 1, 2019; doi:10.1152/ajpheart.00091.2018.

RESEARCH ARTICLE | *Translational Physiology*

Beneficial effects of mesenchymal stem cell delivery via a novel cardiac bioscaffold on right ventricles of pulmonary arterial hypertensive rats

Eric G. Schmuck,[1] Timothy A. Hacker,[1] David A. Schreier,[2] Naomi C. Chesler,[1,2] and Zhijie Wang[2,3]

[1]*Department of Medicine, University of Wisconsin, Madison, Wisconsin;* [2]*Department of Biomedical Engineering, University of Wisconsin, Madison, Wisconsin; and* [3]*Department of Mechanical Engineering, Colorado State University, Fort Collins, Colorado*

Submitted 2 February 2018; accepted in final form 20 February 2019

Schmuck EG, Hacker TA, Schreier DA, Chesler NC, Wang Z. Beneficial effects of mesenchymal stem cell delivery via a novel cardiac bioscaffold on right ventricles of pulmonary arterial hypertensive rats. *Am J Physiol Heart Circ Physiol* 316: H1005–H1013, 2019. First published March 1, 2019; doi:10.1152/ajpheart.00091.2018.—Right ventricular failure (RVF) is a common cause of death in patients suffering from pulmonary arterial hypertension (PAH). The current treatment for PAH only moderately improves symptoms, and RVF ultimately occurs. Therefore, it is necessary to develop new treatment strategies to protect against right ventricle (RV) maladaptation despite PAH progression. In this study, we hypothesize that local mesenchymal stem cell (MSC) delivery via a novel bioscaffold can improve RV function despite persistent PAH. To test our hypothesis, we induced PAH in adult rats with SU5416 and chronic hypoxia exposure; treated with rat MSCs delivered by intravenous injection, intramyocardial injection, or epicardial placement of a bioscaffold; and then examined treatment effectiveness by in vivo pressure-volume measurement, echocardiography, histology, and immunohistochemistry. Our results showed that compared with other treatment groups, only the MSC-seeded bioscaffold group resulted in RV functional improvement, including restored stroke volume, cardiac output, and improved stroke work. Diastolic function indicated by end-diastolic pressure-volume relationship was improved by the local MSC treatments or bioscaffold alone. Cardiomyocyte hypertrophy and RV fibrosis were both reduced, and von Willebrand factor expression was restored by the MSC-seeded bioscaffold treatment. Overall, our study suggests a potential new regenerative therapy to rescue the pressure-overload failing RV with persistent pulmonary vascular disease, which may improve quality of life and/or survival of PAH patients.

NEW & NOTEWORTHY We explored the effects of mesenchymal stem cell-seeded bioscaffold on right ventricles (RVs) of rats with established pulmonary arterial hypertension (PAH). Some beneficial effects were observed despite persistent PAH, suggesting that this may be a new therapy for RV to improve quality of life and/or survival of PAH patients.

cardiac patch; paracrine effect; pulmonary hypertension; regenerative medicine; right heart

INTRODUCTION

Right ventricular failure (RVF) is a common cause of death in patients suffering from chronic pulmonary pressure overload caused by pulmonary arterial hypertension (PAH), an incurable, rapidly developing fatal disease (57). While current treatments for PAH focus on pulmonary vascular endothelial dysfunction and pulmonary arterial vasoconstriction, the clinical successes with these therapies only moderately improve symptoms, and the gradual deterioration in right ventricle (RV) function remains severe, so that organ transplantation is often the last resort (52). The unmet need to rescue the failing right heart necessitates new treatment strategies to protect against RV maladaptation and reduce patient mortality.

Studies of stem cell therapy on PAH have reported improvements in RV functions due to ameliorated pulmonary vascular remodeling (3, 43, 45, 47, 49, 51, 65) and have been recently reviewed (54). Biodistribution studies of intravenously administered cells reveal that most of the cells traffic to the lungs rather than to the heart (3, 43), thus further suggesting that the therapeutic benefit mainly arises from the recovery of the pulmonary disease. However, all of these studies employed a rat model of PAH induced by monocrotaline (MCT) injection, which lacks angio-obliteration formation in the pulmonary vasculature, a hallmark of PAH in humans. In addition, MCT can result in confounding side effects, including myocarditis of the left and right ventricles (44). Moreover, the therapeutic effects of stem cells in lungs are not completely clear and with uncertain physiological relevance (46, 54).

To date, only a limited number of studies have examined stem cell therapy specific for the failing RV. These studies have involved the use of mesenchymal stem cells (MSCs) in a neonatal porcine model (62), cardiac progenitor cells (CPCs) in a juvenile athymic rat model (2), and human umbilical cord blood-derived mononuclear cells (UCBMNC) in athymic nude mice model (38). Interestingly, all of these studies adopted pulmonary artery banding to induce pressure overload [acutely (62) or chronically (2, 38)] in the RV and delivered stem or progenitor cells directly into the RV by intramyocardial injections. To our knowledge, no study has investigated the therapeutic effect of stem cells in a persistent pressure-overloaded RV due to PAH, an acquired, adult disease.

From the research on left ventricle (LV), we have learned that delivery of cellular therapies to the myocardium is complicated by the contractile nature of the heart. Tracking of cells administered either systemically (intravenously or intracoronarily or locally (intramuscularly or intramyocardially) has demonstrated poor myocardial retention (20–22, 41). Systemic, as well as local, IM delivery of cells has been shown to result in a rapid washout of the cells to the lungs, liver, and spleen (8, 20, 40). Therefore, despite numerous positive results

Address for reprint requests and other correspondence: Z. Wang, Colorado State Univ., 1301 Campus Delivery, Fort Collins, CO 80523 (e-mail: Zhijie.Wang@colostate.edu).

from prior LV studies, it is believed that the low engraftment rate restricts the treatment effectiveness, and other delivery approach, such as bioscaffold patches, may fulfill the clinical need (67). To improve cell retention and localize biodistribution to the myocardium, a novel bioscaffold [cardiac fibroblast-derived extracellular matrix (CF-ECM)] has been tested as a cell retention agent (42). CF-ECM is a cell-secreted matrix that self-attaches to the epicardial surface of the ventricle and has been shown to effectively transfer MSCs to the LV (42).

The goal of the present study is to explore the treatment effects of MSCs with various delivery methods for RVF secondary to PAH using a well-established adult rat model of PAH, the SU5416+hypoxia (SuHx) model (5, 44). We hypothesize that local MSC delivery via CF-ECM will improve RV performance despite persistent pressure overload. Our results demonstrated that MSC-seeded bioscaffold improved RV function despite persistent pressure overload, whereas this effect was absent in both intravenous and intramyocardial MSC injection groups.

MATERIALS AND METHODS

Animal handling. All procedures were approved by University of Wisconsin Institutional Animal Care and Use Committee. To induce irreversible PAH (1, 11), 5–6-wk-old male Sprague-Dawley rats (Harlan, Indianapolis, IN) were treated with a single subcutaneous injection of SUGEN (SU5416; Millipore Sigma) at a dose of 20 mg/kg and then housed in hypoxia chamber (10% O_2) for 4 wk and in normal room air for another 2 wk (5). SUGEN/SU5416 is a vascular endothelial growth factor (VEGF) receptor inhibitor. The PAH rats were randomized and then treated with MSCs via three delivery methods (intravenous, intramyocardial, and cell-seeded bioscaffold). Intravenous and intramyocardial MSC treatment groups were tested, being common delivery methods in the field (67). Finally, a group of animals were treated with the bioscaffold alone to test the effect of the CF-ECM material on RV recovery. Three weeks posttreatment, all groups were examined for RV function and structure, as described below. Identical measurements were performed in healthy rats and untreated PAH rats at a similar age.

Bioscaffold manufacturing and MSC delivery. A novel bioscaffold was employed for RV MSC delivery using previously described methods (42). Briefly, to induce bioscaffold formation, rat cardiac fibroblasts from passages 2 and 3 were plated at a density of ~1.1×10^5 to 2.2×10^5 per cm^2 in high-glucose DMEM + 10% FBS and 1% penicillin/streptomycin for 10–14 days. Then, cardiac fibroblasts and secreted ECM were incubated with 2 mM EDTA solution at 37°C. To remove remaining cells, the bioscaffold sheet was incubated in alternating hyper/hypotonic Tris-buffered saline followed by 48-h incubation with 1% tri-*n*-butyl-phosphate (TnBp) at 4°C with constant agitation. Contaminating DNA was removed by 1-h incubation with DNase 1. Finally, the bioscaffold was rinsed in 100% ethanol followed by washes with sterile water and PBS.

EGFP+rMSCs (cat. no. RASMX-0110) were purchased from Cyagen Biosciences (Santa Clara, CA) and expanded per the manufacturers' protocols. 2×10^6 cells were suspended in 50 μl of Plasmalyte A and seeded on top of the bioscaffold for 2 h just before implantation. After the rat was anesthetized and the chest was open, scaffolds with and without MSC seeding were gently rinsed in Plasmalyte A, inverted, and placed on the right heart (cell side down). The bioscaffold used in this study is self-adhesive; thus, it eliminates the need to glue or suture the patch onto the RV (42). In another group of rats, 2×10^6 MSCs were delivered to the RV by direct intramyocardial injections at two or three sites. In a third group of rats, the same amount of MSCs was injected systemically via a jugular vein.

In vivo pressure-volume loop measurements. In vivo RV pressure-volume (PV) relationships were obtained using similar methods as previously (31, 60, 61). Briefly, rats were anesthetized with urethane (1.2 g/kg), intubated, and ventilated followed by a ventral midline skin incision. After the RV was exposed, a 1.9-Fr admittance polyvinyl catheter (Transonic Scisense, Ithaca, NY) was introduced into the apex of the RV. The steady-state signals were recorded, and then at least three transient (~1 s) preload reductions were induced by entrapping and occluding the inferior vena cava with a suture. The end-diastolic pressure-volume relationship (EDPVR) and two preload independent contractility indices—end-systolic pressure-volume relationship (ESPVR, or Ees) and preload-recruitable stroke work (PRSW)—were derived from the occlusion PV loops. Data were recorded and analyzed using commercially available software (Notocord Systems, Croissy Sur Seine, France). Animals were euthanized by exsanguination, and the RV free wall, LV, and septum were harvested and weighed. RV hypertrophy was assessed by *1*) the Fulton index as the weight ratio of RV and (LV+septum) and *2*) the ratio of RV weight to body weight (RV/BW).

Hemodynamic data analysis. The PV loops were recorded, and at least 10 consecutive cardiac cycles free of extra systolic beats were selected and used for the analysis (60). Standard hemodynamic variables, including heart rate (HR), RV systolic pressure (RVSP), total pulmonary vascular resistance (TPVR, estimated as RVSP/cardiac output) and common RV function parameters, such as stroke volume (SV), cardiac output (CO), ejection fraction (EF), and effective arterial elastance (Ea) were obtained from the steady-state PV loops. RV contractile function was quantified in these indices: stroke work (SW), slope of ESPVR/Ees, PRSW, dP/dt_{max}, and preload adjusted maximal power (PAMP, estimated as maximal power PWRmax divided by end-diastolic volume) (53). RV diastolic function was further measured by dP/dt_{min}, end-diastolic volume (EDV), and the slope of EDPVR. Finally, the RV-pulmonary vascular interaction was evaluated by ventricular-vascular coupling (VVC), a well-accepted parameter for RV function assessment in animal and clinical studies (15, 48), as *1*) the ratio of Ees to Ea and *2*) the ratio of SV/ESV, where ESV is the end-systolic volume. All parameters were analyzed and exported directly by Notocord or calculated as described above.

Echocardiography. In the bioscaffold-treated rats with and without MSCs seeding, transthoracic echocardiography was performed with a 17.5-MHz transducer (RMV 707B; Visual Sonics, Toronto, ON, Canada) to assess RV function at baseline (*week 0*), after PAH development (*week 6*) and 3 wk after treatment (*week 9*), using methods previously described (13). Typical geometrical and functional parameters of the RV, including fraction shortening (FS) and tricuspid annular plane systolic excursion (TAPSE) indicative of the systolic function, were measured in the rats (25).

Histology and immunohistochemistry. After euthanasia, RVs were harvested, fixed in 10% formalin, and stained with H&E and Sirius Red (37). RV cardiomyocyte morphology was measured by the cell area under the cross-sectional orientation and the cell width under the longitudinal orientation (60). RV fibrosis was measured by the collagen area percentage in the tissue. To quantify myocardial perfusion, immunohistochemistry was performed to examine the expression levels of von Willebrand factor (vWF) using a similar method, as described previously (60).

Statistics. All parameters derived from invasive pressure-volume loops, RV tissue hypertrophy, histology, and immunohistochemistry were analyzed by one-way ANOVA with a Fisher's least significant difference post hoc test. RV echocardiography was analyzed with repeated-measures, one-way ANOVA with a Tukey's post hoc analysis. All analyses were performed with Prism 7 (GraphPad, San Diego, CA). All results are expressed as means ± SD. $P < 0.05$ was considered statistically significant.

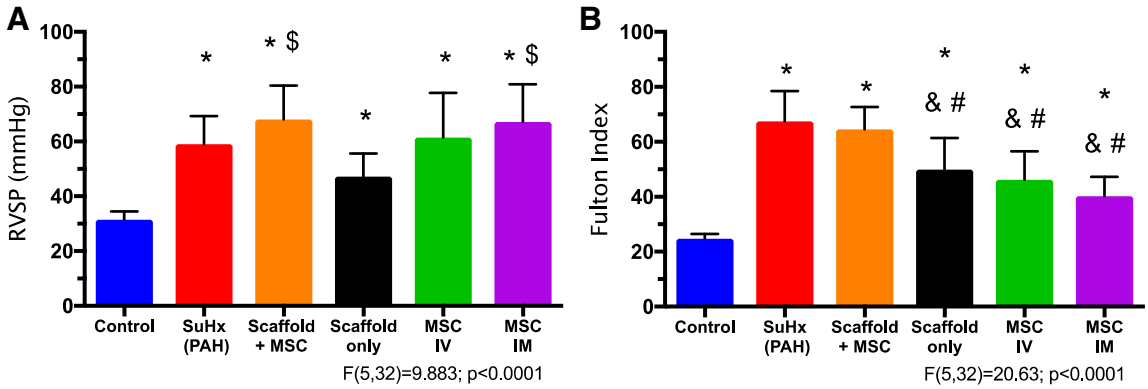

Fig. 1. Right ventricle systolic pressure (RVSP; *A*) and hypertrophy index (Fulton Index; *B*) measurements in the experimental groups. Results are shown as means ± SD; $n = 8$ for control, PAH, and Scaffold+mesenchymal stem cell (MSC) groups, and $n = 5$ for scaffold only, intravenous (IV) MSC, and intramyocardial (IM) MSC groups. *$P \leq 0.05$ vs. control; #$P \leq 0.05$ vs. PAH; $$P \leq 0.05$ vs. scaffold only; &$P \leq 0.05$ vs. Scaffold+MSC.

RESULTS

Persistent RV pressure overload and tissue hypertrophy in all treatment groups. We examined the degree of PAH by the changes in pulmonary arterial pressure. As shown in Fig. 1, the RVSP was significantly elevated in the SuHx (PAH) group, and the elevation in RVSP was not reduced by any of the treatment groups. The examination on the entire pulmonary arterial afterload, such as Ea and total pulmonary vascular resistance (Table 1), confirmed a similar trend of persistent increase in RV afterload in all treatment groups. These results indicate that PAH was not alleviated by any treatment group.

RV hypertrophy at the tissue level was quantified by the Fulton Index (Fig. 1) and the ratio of RV tissue weight to body weight (RV/BW; Table 1). All treatment groups resulted in milder but persistent hypertrophy, except for the MSC-seeded bioscaffold treatment group (Fig. 1).

MSC-seeded bioscaffold treatment improved overall RV function. Even with persistent PAH and RV pressure overload, improvements in RV function were observed with MSC-seeded bioscaffold treatment. In contrast, the therapeutic effect was absent or marginal in all other treatment groups. As shown in Fig. 2, we have observed significant reduction in RV SV and CO in the untreated PAH group compared with control, and the restoration of them to control levels occurred only in the MSC-seeded bioscaffold treatment group ($P < 0.05$; Fig. 2, *A* and *B*). A trend toward improved RV EF was observed in the bioscaffold-treated groups (with and without MSCs), but the changes were insignificant (Table 1). We did not observe marked differences in HR, EDV, or ESV between treatment groups (Table 1).

MSC-seeded bioscaffold treatment differently affected the contractility indices. We examined the RV contractile function by SW, Ees, PRSW, PAMP, and dP/dt_{max}. We found that while PAH development tended to increase RV SW, the MSC-seeded bioscaffold treatment further increased the SW significantly ($P < 0.05$, Fig. 2*C*), suggesting an enhanced overall RV contractility. In contrast, no other treatment group increased the RV SW compared with the untreated PAH group (Fig. 2*C*). Furthermore, because SW is preload-dependent, we examined another relevant but preload-independent contractility index, PAMP (53). We observed similarly increased PAMP with the MSC-seeded bioscaffold treatment ($P < 0.05$, Table 1).

PRSW and dP/dt_{max} were consistently increased in all PAH groups, except for the scaffold-only treatment group, and there were no significant alterations in these parameters with any of the treatment (Table 1). In the Ees measurement, the untreated PAH group and MSC-seeded bioscaffold-treated group had

Table 1. *RV tissue hypertrophy and hemodynamic measurements in all experimental groups*

	Control	PAH	Scaffold+MSCs	Scaffold Only	IV MSCs	IM MSCs
RV/BW	0.58 ± 0.03	1.58 ± 0.23*	1.45 ± 0.18*	1.28 ± 0.35*	1.05 ± 0.28*†	0.92 ± 0.18*†
tPVR, mmHg·min^{-1}·ml	0.3 ± 0.1	0.8 ± 0.3*	0.7 ± 0.2*	0.6 ± 0.2	0.9 ± 0.2	1.0 ± 0.3*
RV EDV, μl	352 ± 50	391 ± 118	474 ± 68	380 ± 84	407 ± 36	393 ± 36
RV ESV, μl	114 ± 80	199 ± 117	162 ± 83	128 ± 58	182 ± 69	191 ± 43
EF, %	73 ± 15	49 ± 16*	63 ± 12	66 ± 14	55 ± 15	51 ± 7*
HR, bpm	320 ± 40	335 ± 25	332 ± 39	337 ± 49	345 ± 31	336 ± 23
PAMP, mWatt/μl	0.67 ± 0.65	0.60 ± 0.35	1.46 ± 1.21*†	2.12 ± 3.01	0.38 ± 0.18	0.78 ± 0.57
dP/dt_{min}, mmHg/s	−1,325 ± 300	−3,580 ± 1,186*	−3,033 ± 575*	−2,440 ± 897*	−3,147 ± 933*	−2,853 ± 519*
dP/dt_{max}, mmHg/s	2,544 ± 681	4,502 ± 580*	4,854 ± 992*	4,213 ± 2,400	4,642 ± 529*	4,602 ± 1,140*
PRSW	26 ± 10	68 ± 20*	63 ± 21*	67 ± 34	56 ± 17*	58 ± 25*
Ees, mmHg/μl	0.26 ± 0.09	0.44 ± 0.18*	0.46 ± 0.13*	0.47 ± 0.10	0.51 ± 0.23	0.32 ± 0.09
Ea, mmHg/μl	0.13 ± 0.03	0.24 ± 0.06*	0.24 ± 0.07*	0.23 ± 0.10	0.28 ± 0.11	0.34 ± 0.11*
VVC, Ees/Ea	2.4 ± 1.3	1.7 ± 0.6	1.8 ± 0.6	2.7 ± 1.6	2.4 ± 1.9	1.0 ± 0.4
VVC, SV/ESV	3.7 ± 2.5	1.3 ± 1.0*	2.1 ± 1.3	2.5 ± 1.6	1.5 ± 1.1*	1.1 ± 0.3*

Values are means ± SD; $n = 8$ for control, PAH and Scaffold+MSCs groups, and $n = 5$ for all other treatment groups. BW, body weight; EDV, end-diastolic volume; EF, ejection fraction; ESV, end-systolic volume; HR, heart rate; PAMP, preload adjusted maximal power; PRSW, preload recruitable stroke work; RV, right ventricle; RV/BW, the ratio of RV tissue weight over body weight; SV, systolic volume; tPVR, total pulmonary vascular resistance; VVC, ventricular-vascular coupling. *$P < 0.05$ vs. control. †$P < 0.05$ vs. PAH.

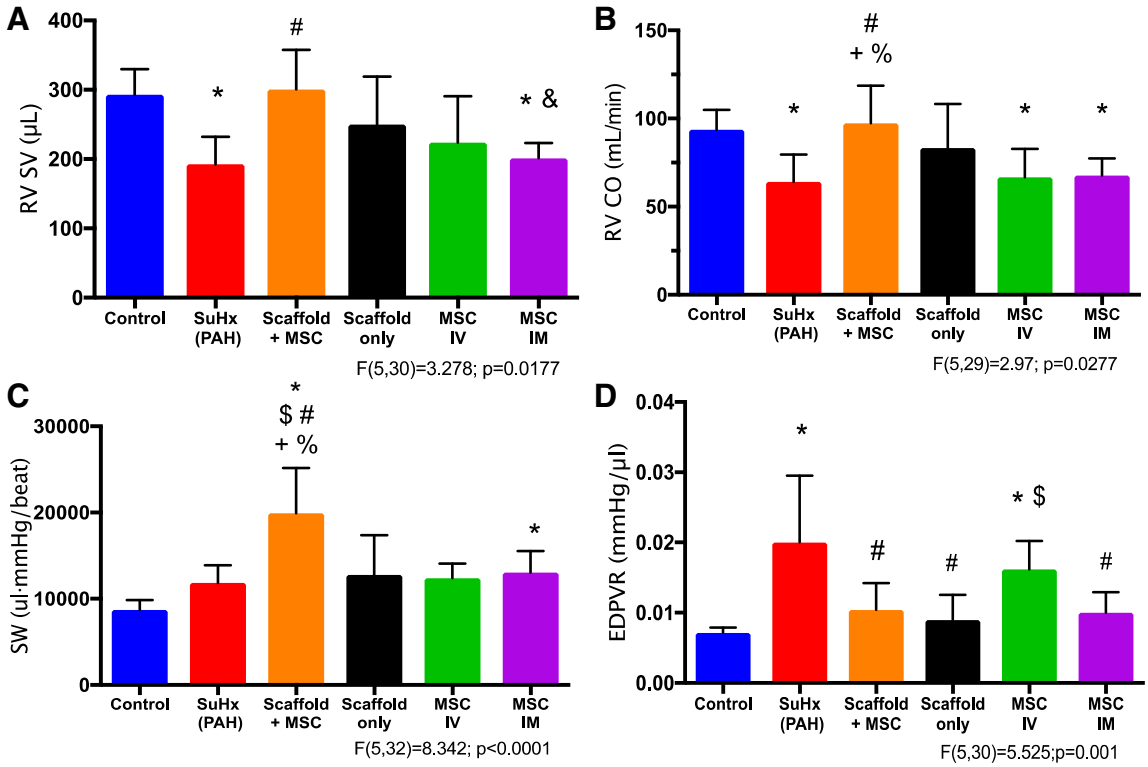

Fig. 2. Right ventricle stroke volume (RV SV; *A*), right ventricle cardiac output (RV CO; *B*), stroke work (SW; *C*), and end-diastolic pressure-volume relation (EDPVR; *D*) measurements in the experimental groups. RV function improvement post-mesenchymal stem cell (MSC)-seeded bioscaffold treatment is evident. Results are shown as means ± SD; $n = 8$ for control, pulmonary arterial hypertension (PAH), and Scaffold+mesenchymal stem cell (MSC) groups, and $n = 5$ for scaffold only, intravenous (IV) MSC and intramyocardial (IM) MSC groups. *$P \leq 0.05$ vs. control; #$P \leq 0.05$ vs. PAH; \$$P \leq 0.05$ vs. scaffold only; &$P \leq 0.05$ vs. Scaffold+MSC; +$P \leq 0.05$ vs. IV MSC; %$P \leq 0.05$ vs. IM MSC.

similarly elevated Ees, but such change was absent in other treatment groups (Table 1). This suggests that with the continuously increased RV afterload (Ea), the MSC-seeded bioscaffold group was able to maintain RV contractility (Ees), while the other treatment groups failed to do so.

Improved RV EDPVR in "local" treatment groups. Diastolic function was examined by EDPVR, RV end-diastolic volume (EDV), and dP/dt_{min}. While PAH led to significantly increased EDPVR, this parameter was reduced to the control levels in all "local" treatment groups ($P < 0.05$, Fig. 2*D*), suggesting an improvement in diastolic function. We did not observe significant changes in RV EDV among all experimental groups (Table 1). Similar to the changes in dP/dt_{max}, dP/dt_{min} (the absolute value) was increased in all diseased groups, and none of the treatment groups affected the increase in dP/dt_{min} (Table 1).

Potential improvement in cardiopulmonary coupling in the bioscaffold treatment groups. Ventricular-vascular coupling (VVC) of the RV was evaluated by two established methods: Ees/Ea and SV/ESV. Because of the large variation in Ees/Ea, we did not observe significant changes in all experimental groups (Table 1). When estimated by SV/ESV ratios, we found that PAH significantly reduced VVC ($P < 0.05$; Table 1), and the reduction in VVC was absent in both bioscaffold treatment groups (with and without MSCs). In contrast, intravenous and intramyocardial MSC groups showed persistently low VVC compared with the control RV ($P < 0.05$, Table 1).

Temporal changes in RVs of the mesenchymal stem cell-seeded bioscaffold or bioscaffold-only treatment groups. We performed serial echocardiography measurements in the rats treated by MSC-seeded bioscaffold and bioscaffold only. We found that RV FS was significantly reduced with the PAH development ($P < 0.05$) and that neither the MSC-seeded bioscaffold treatment nor the bioscaffold-only treatment rescued this reduction (Tables 2 and 3). RV chamber size was significantly enlarged with PAH development, and neither MSC-seeded bioscaffold nor bioscaffold-only treatments ameliorated the enlargement ($P < 0.05$, Tables 2 and 3). Finally, we did not observe significant changes in TAPSE in either the MSC-seeded bioscaffold or bioscaffold-only group.

Table 2. *Echocardiography measurements at multiple time points for the same rats treated with MSC-seeded bioscaffold*

	Baseline	PAH	Scaffold+MSCs
FS	0.57 ± 0.07	0.32 ± 0.11*	0.30 ± 0.09*
TAPSE, mm	1.87 ± 0.2	1.58 ± 0.36	2.15 ± 0.58
RV ID, s, mm	1.60 ± 0.21	2.82 ± 0.28*	3.15 ± 0.57*
RV ID, d, mm	2.87 ± 0.26	3.88 ± 0.35*	4.22 ± 0.52*
RV ID/LV ID, s	0.28 ± 0.05	0.45 ± 0.06*	0.43 ± 0.06*
RV ID/LV ID, d	0.38 ± 0.03	0.47 ± 0.04*	0.47 ± 0.04*

Values are means ± SD; $n = 8$. Baseline, before SuHx treatment; d, diastole; FS, fractional shortening; LV ID, LV inner diameter; PAH, pulmonary arterial hypertension after 6 wk of SuHx treatment; RV ID, RV inner diameter; Scaffold+MSCs, after 3 wk of MSC-seeded bioscaffold treatment; s, systole; TAPSE, tricuspid annular plane systolic excursion. All parameters were measured at three time points in the same animal except for TAPSE, with which the measurement was unavailable for *rat 3* during the baseline and PAH measurements. *$P < 0.05$ vs. baseline.

Table 3. *Echocardiography measurements at multiple time points for the same rats treated with bioscaffold alone*

	Baseline	PAH	Scaffold Only
FS	0.42 ± 0.10	0.29 ± 0.09*	0.27 ± 0.05*
TAPSE, mm	2.27 ± 0.7	2.40 ± 0.25	1.88 ± 0.62
RV ID, s mm	1.75 ± 0.35	2.62 ± 0.36*	2.81 ± 0.52*
RV ID, d mm	2.69 ± 0.49	3.53 ± 0.61	3.66 ± 0.55*
RV ID/LV ID, s	0.28 ± 0.06	0.35 ± 0.05	0.35 ± 0.05*
RV ID/LV ID, d	0.36 ± 0.07	0.40 ± 0.07	0.39 ± 0.04

Values are means ± SD; $n = 6$. Baseline, before SuHx treatment; d, diastole; FS, fractional shortening; LV ID, left ventricle inner diameter; PAH, pulmonary arterial hypertension after 6-wk SuHx treatment; Scaffold Only, after 3-wk bioscaffold only treatment; RV ID, right ventricle inner diameter; s, systole; TAPSE, tricuspid annular plane systolic excursion. All parameters were measured at three time points in the same animal. *$P < 0.05$ vs. baseline.

Structural changes in RVs of the mesenchymal stem cell-seeded bioscaffold treatment group. We examined RV collagen content and RV cardiomyocyte morphology with routine histology staining. PAH led to increases in RV collagen content, and the MSC-seeded bioscaffold mildly reduced the collagen deposition in the diseased RVs ($P < 0.05$, Fig. 3*A*). PAH also led to RV cardiomyocyte enlargement evidenced by increased cell size and width. Interestingly, the degree of RV cardiomyocyte enlargement was reduced by the MSC-seeded bioscaffold treatment ($P < 0.05$, Fig. 3, *B* and *C*).

We further measured the expression of vWF in blood vessels in these RVs. As vWF is expressed by healthy endothelial cells, the amount of vWF expression is a good indicator of coronary artery perfusion (64, 68). As shown in Fig. 4, PAH led to decreased vWF expression in the RV, and the MSC-seeded bioscaffold treatment reversed the reduction ($P < 0.05$). Thus, myocardial perfusion is likely improved with the treatment.

DISCUSSION

In the current study, we investigated the therapeutic effects of MSCs on pressure-overloaded RVs via different delivery methods (intravenous, intramyocardial, and cell-seeded bioscaffold). We found that local MSC delivery via engineered bioscaffolds significantly improved RV performance, as evidenced by restored CO and SV. In addition, overall RV contractility (SW and PAMP) was enhanced and diastolic function (EDPVR) was improved by this treatment. Biological examination suggests that the mechanism of these beneficial effects may be a result of reduced RV fibrosis and cardiomyocyte hypertrophy, as well as increased coronary perfusion. To our knowledge, this is the first study to investigate MSC therapy for adult RVF secondary to PAH, as well as the first study to demonstrate beneficial effects of MSCs on failing RVs delivered via a novel self-adherent cardiac bioscaffold.

MSC-seeded bioscaffold improves global RV function despite persistent pressure overload. This study suggests that, despite persistent pressure overload, treatment with MSC-seeded bioscaffold improves global RV function by restoring SV and CO to control levels. The overall improvement may be explained, in part, by the increased SW and PAMP, the contractility indices of the total work power generated per heartbeat. Cardiac contractility is the intrinsic ability of the heart to generate force (24). It has been previously reported that in the infarcted LV, IM delivery of MSCs improves cardiac contractility (41, 63). The exact mechanism by which MSCs improve cardiac contractility in the LV following ischemic injury is not fully known, but reports of neoangiogenesis and reduction in scar size have been cited (14, 18, 26, 50). Although stem cells have been reported to improve RV function in volume-overload or pressure-overload RV models in neonatal sheep and pigs (9, 62, 66), to our knowledge, this study is the first to investigate the effect of RV-specific MSC therapy using the SuHx PAH model.

In this study, we chose to test both conventional (intravenous, intramyocardial) and nascent (bioscaffold) cell delivery methods to determine the optimal cell delivery method. While intravenous and intramyocardial cell deliveries have been widely tested in various cardiac disease models, we found that they failed to improve RV function or reverse deleterious remodeling. In fact, intravenous MSC therapy in MCT-induced PAH rats has yielded mixed results (45, 49, 51). Although the efficacy and safety of MSC therapy to reverse pulmonary vascular remodeling remain unclear (46), our results suggest that intravenous delivery of MSCs is not optimal for RV failure. Unexpectedly, our results showed that not only did intramyocardial MSC treatment fail to improve RV function, but instead, resulted in the worst RV contractility (Ees) and VVC among all treatment groups (Table 1). While it is unclear why intramyocardial MSC therapy resulted in worsening RV function, it is likely that rapid washout of MSCs coupled with potential damage caused by the act of injecting cells into an already weakened RV may have contributed to this result. Finally, the bioscaffold-only treatment was tested. Interestingly, the bioscaffold alone improved diastolic func-

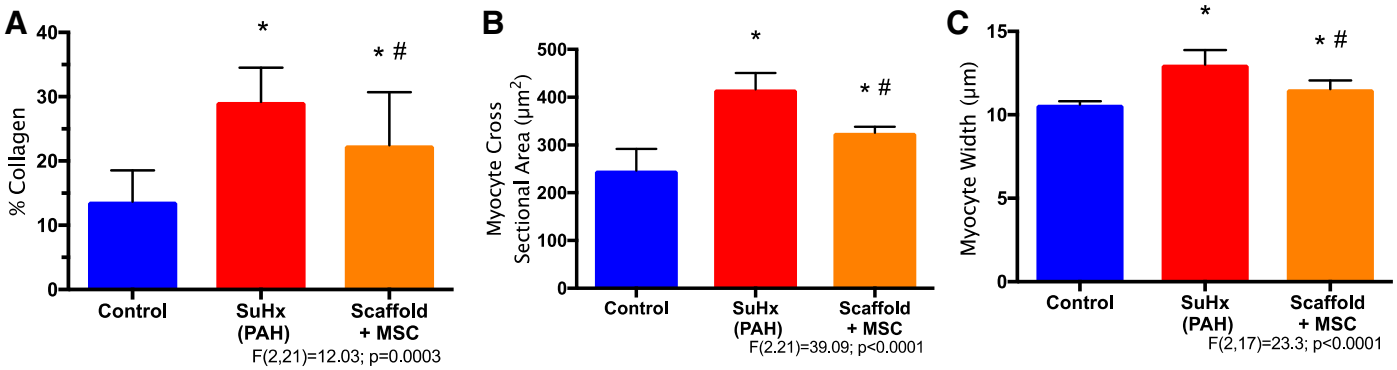

Fig. 3. Right ventricle (RV) histology measurements on collagen area percentage (*A*), cardiomyocyte cross-sectional area (*B*), and cardiomyocyte width (*C*) in control, pulmonary arterial hypertension (PAH) and mesenchymal stem cell (MSC)-seeded bioscaffold treatment groups, respectively. Results are shown as means ± SD; $n = 8$ per group. *$P \leq 0.05$ vs. control; #$P \leq 0.05$ vs. PAH.

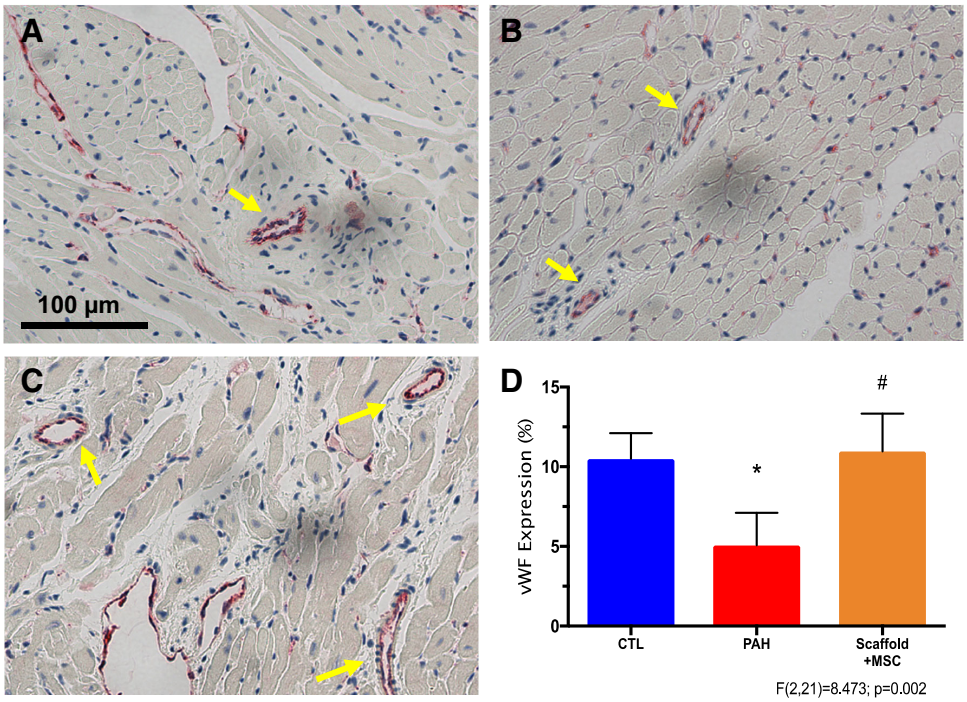

Fig. 4. Right ventricle (RV) myocardial perfusion measurement by von Willebrand factor (vWF) expression. *A–C*: representative images of RVs stained for vWF expression (red color) in control, PAH, and MSC-seeded bioscaffold treatment groups, respectively. Arrows indicate blood vessels found in RV tissues. *D*: vWF expression level changes in these RVs. Results are shown as means ± SD; $n = 8$ per group. *$P \leq 0.05$ vs. control; #$P \leq 0.05$ vs. PAH.

tion, as shown by a reduction in EDPVR (Fig. 2*D*). However, other key functional improvements, such as the restoration of SV, CO, and enhanced SW were absent. Thus, we attribute these beneficial effects of the MSC-seeded bioscaffold to the MSCs rather than the bioscaffold itself.

Potential mechanism of MSC-seeded bioscaffold treatment: promoting angiogenesis and reducing fibrosis in the RV. While the exact mechanism by which MSCs convey benefit is still debated, evidence strongly suggests that paracrine signaling through cytokines, growth factors, and microvesicles is involved. Paracrine signaling has been shown to promote angiogenesis (16, 19, 23, 35), beneficially modulate the immune system (6, 10, 36), and reduce fibrosis (28, 34). All three of these MSC properties could be beneficial to the RV. Capillary rarefaction, resulting in reduced blood flow, is a well-documented phenomenon in the RVF (56, 58, 59). We observed increased vWF expression in the RV, which may improve cardiac perfusion (Fig. 4), suggesting that the proangiogenic properties of MSCs may be a potential mechanism leading to improved RV function. Our results also indicated that treatment with MSC-seeded bioscaffold reduces RV fibrosis (Fig. 3*A*), which is consistent with previous findings in failing LVs (30). Additionally, histological examination showed ameliorated cardiomyocyte hypertrophy with the treatment (Fig. 3, *B* and *C*). This finding is also consistent with previous reports that MSCs reduce myocyte hypertrophy in vitro (7), as well as in vivo, in a myocardial infarction rat model (33), suggesting another potential mechanism by which MSCs restore cardiomyocytes at the cellular level.

Implications in regenerative therapy for RV failure. Although the aim of regenerative therapy is to halt/reverse RV failure, an unsolved issue in the field is the definition of RV failure, which is likely to be distinct from LV failure (12). Presently, there is no clear clinical definition of RV failure, probably due to the lack of detailed cellular and molecular mechanisms to explain RVF (55, 57). RV failure has been identified by reduction in CO, SV, and/or EF, RV wall dilation, decreased contractility, or VVC. But not all of these parameters are able to consistently predict RV failure: in some cases, RV contractility increases as an adaptive response, but SV or CO decreases, fulfilling a definition of failure (29); in other cases, the failing RV has reduced EF and diastolic dysfunction yet preserved CO (39). Therefore, it is essential to understand the progression of RV failure to better guide therapeutic goals.

An emerging area in the regenerative medicine arises from the discovery of beneficial effects of stem cells from their secretome or exosomes (17). Exosomes are extracellular vesicles secreted from stem cells or stem cell-derived cardiomyocytes, and they have been reported to reduce the size of infarctions and improve organ function (4, 27, 32). Despite the benefits, the mechanism of the exosomes in the failing LVs has not been fully clarified. In the present study, it is also possible that the RV improvement, including the biological changes, was a result of the paracrine effects of exosomes from the MSCs. Because of the potentially different mechanisms between LV and RV failure, future investigations should consider the unique components of the exosomes that are specific for failing RVs.

Limitations. There are several limitations in the present study. First, we have not directly measured the pulmonary vascular remodeling by lung histology or immunohistochemistry. Instead, we indirectly infer that pulmonary arterial afterload was not altered by functional parameters (Ea and tPVR). Second, the measurement of EF was not carried out by cardiac MRI, which is considered the gold standard for this functional parameter. Third, the organ level measurement of RV hypertrophy was not consistent with the microscopic level measurement. It is known that the entire organ wet weight is dependent on multiple factors, and single myocyte hypertrophy is only one of them. Future studies should distinguish the cause for the difference between organ-level and cellular-level measurements of muscle hypertrophy. Fourth, we did not fully examine

the functional and structural changes in every control group as we performed for the MSC-seeded bioscaffold group. For the treatment groups with "absent" functional improvements, we did not perform histological examination or temporal echocardiography. As a result, it is not fully clear whether and to what extent the bioscaffold itself may alter the remodeling of the RV, or whether the bioscaffold has an impact on the MSCs besides the proposed "vehicle" function. Finally, although we observed some beneficial effects of the MSC-seeded bioscaffold treatment, the improvement is not optimal. This may be part of the reason that the changes in different contractility indices were not identical. Future research should seek to optimize the treatment with varied dose or timing of delivery of MSCs.

In summary, our results showed beneficial effects of localized MSC delivery to the failing RV via a novel bioscaffold. The restoration of SV and CO and improved SW and PAMP indicated a global improvement in the RV function. Biological examination showed that the degrees of cardiomyocyte hypertrophy and RV fibrosis were reduced, and coronary perfusion was increased by the MSC-seeded bioscaffold treatment. However, how exactly the local MSCs delivery via a bioscaffold led to RV myocardium recovery awaits further investigation. Refinement of the cell-seeded bioscaffold treatment may eventually provide novel treatment for RVF secondary to PAH and improve quality of life for PAH patients, even under persistent pulmonary vascular disease.

ACKNOWLEDGMENTS

We thank Dr. Guoqing Song and Gaoussou M. Diarra for assistance with surgical preparation and data acquisition and Dr. Jill Koch and Allison Rodgers for assistance with echocardiography data acquisition. We thank Michael Nguyen-Truong for assistance with immunohistochemistry image analysis.

GRANTS

This study was partly supported by National Heart, Lung, and Blood Institute Grant R01-HL-086939 (to N. C. Chesler).

DISCLOSURES

E. G. Schmuck has ownership and financial interest in Cellular Logistics, Inc.

AUTHOR CONTRIBUTIONS

E.G.S. and Z.W. conceived and designed research; E.G.S., T.A.H., D.A.S., and Z.W. performed experiments; E.G.S., T.A.H., D.A.S., and Z.W. analyzed data; E.G.S., T.A.H., N.C., and Z.W. interpreted results of experiments; E.G.S. and Z.W. prepared figures; E.G.S. and Z.W. drafted manuscript; E.G.S., T.A.H., N.C., and Z.W. edited and revised manuscript; E.G.S., T.A.H., and Z.W. approved final version of manuscript.

REFERENCES

1. **Abe K, Toba M, Alzoubi A, Ito M, Fagan KA, Cool CD, Voelkel NF, McMurtry IF, Oka M.** Formation of plexiform lesions in experimental severe pulmonary arterial hypertension. *Circulation* 121: 2747–2754, 2010. doi:10.1161/CIRCULATIONAHA.109.927681.
2. **Agarwal U, Smith AW, French KM, Boopathy AV, George A, Trac D, Brown ME, Shen M, Jiang R, Fernandez JD, Kogon BE, Kanter KR, Alsoufi B, Wagner MB, Platt MO, Davis ME.** Age-dependent effect of pediatric cardiac progenitor cells after juvenile heart failure. *Stem Cells Transl Med* 5: 883–892, 2016. doi:10.5966/sctm.2015-0241.
3. **Angelini A, Castellani C, Ravara B, Franzin C, Pozzobon M, Tavano R, Libera LD, Papini E, Vettor R, De Coppi P, Thiene G, Vescovo G.** Stem-cell therapy in an experimental model of pulmonary hypertension and right heart failure: role of paracrine and neurohormonal milieu in the remodeling process. *J Heart Lung Transplant* 30: 1281–1293, 2011. doi:10.1016/j.healun.2011.07.017.
4. **Bian S, Zhang L, Duan L, Wang X, Min Y, Yu H.** Extracellular vesicles derived from human bone marrow mesenchymal stem cells promote angiogenesis in a rat myocardial infarction model. *J Mol Med (Berl)* 92: 387–397, 2014. doi:10.1007/s00109-013-1110-5.
5. **Bogaard HJ, Natarajan R, Henderson SC, Long CS, Kraskauskas D, Smithson L, Ockaili R, McCord JM, Voelkel NF.** Chronic pulmonary artery pressure elevation is insufficient to explain right heart failure. *Circulation* 120: 1951–1960, 2009. doi:10.1161/CIRCULATIONAHA.109.883843.
6. **Bouchlaka MN, Moffitt AB, Kim J, Kink JA, Bloom DD, Love C, Dave S, Hematti P, Capitini CM.** Human mesenchymal stem cell-educated macrophages are a distinct high IL-6-producing subset that confer protection in graft-versus-host-disease and radiation injury models. *Biol Blood Marrow Transplant* 23: 897–905, 2017. doi:10.1016/j.bbmt.2017.02.018.
7. **Cai B, Tan X, Zhang Y, Li X, Wang X, Zhu J, Wang Y, Yang F, Wang B, Liu Y, Xu C, Pan Z, Wang N, Yang B, Lu Y.** Mesenchymal stem cells and cardiomyocytes interplay to prevent myocardial hypertrophy. *Stem Cells Transl Med* 4: 1425–1435, 2015. doi:10.5966/sctm.2015-0032.
8. **Caveliers V, De Keulenaer G, Everaert H, Van Riet I, Van Camp G, Verheye S, Roland J, Schoors D, Franken PR, Schots R.** In vivo visualization of 111In labeled CD133+ peripheral blood stem cells after intracoronary administration in patients with chronic ischemic heart disease. *Q J Nucl Med Mol Imaging* 51: 61–66, 2007.
9. **Davies B, Elwood NJ, Li S, Cullinane F, Edwards GA, Newgreen DF, Brizard CP.** Human cord blood stem cells enhance neonatal right ventricular function in an ovine model of right ventricular training. *Ann Thorac Surg* 89: 585–593.4, 2010. doi:10.1016/j.athoracsur.2009.10.035.
10. **Eggenhofer E, Hoogduijn MJ.** Mesenchymal stem cell-educated macrophages. *Transplant Res* 1: 12, 2012. doi:10.1186/2047-1440-1-12.
11. **Firth AL, Mandel J, Yuan JX.** Idiopathic pulmonary arterial hypertension. *Dis Model Mech* 3: 268–273, 2010. doi:10.1242/dmm.003616.
12. **Friedberg MK, Redington AN.** Right versus left ventricular failure: differences, similarities, and interactions. *Circulation* 129: 1033–1044, 2014. doi:10.1161/CIRCULATIONAHA.113.001375.
13. **Golob MJ, Tian L, Wang Z, Zimmerman TA, Caneba CA, Hacker TA, Song G, Chesler NC.** Mitochondria DNA mutations cause sex-dependent development of hypertension and alterations in cardiovascular function. *J Biomech* 48: 405–412, 2015. doi:10.1016/j.jbiomech.2014.12.044.
14. **Gomes SA, Rangel EB, Premer C, Dulce RA, Cao Y, Florea V, Balkan W, Rodrigues CO, Schally AV, Hare JM.** S-nitrosoglutathione reductase (GSNOR) enhances vasculogenesis by mesenchymal stem cells. *Proc Natl Acad Sci USA* 110: 2834–2839, 2013. doi:10.1073/pnas.1220185110.
15. **Guihaire J, Haddad F, Boulate D, Decante B, Denault AY, Wu J, Hervé P, Humbert M, Dartevelle P, Verhoye JP, Mercier O, Fadel E.** Non-invasive indices of right ventricular function are markers of ventricular-arterial coupling rather than ventricular contractility: insights from a porcine model of chronic pressure overload. *Eur Heart J Cardiovasc Imaging* 14: 1140–1149, 2013. doi:10.1093/ehjci/jet092.
16. **Gupta PK, Chullikana A, Parakh R, Desai S, Das A, Gottipamula S, Krishnamurthy S, Anthony N, Pherwani A, Majumdar AS.** A double blind randomized placebo controlled phase I/II study assessing the safety and efficacy of allogeneic bone marrow derived mesenchymal stem cell in critical limb ischemia. *J Transl Med* 11: 143, 2013. doi:10.1186/1479-5876-11-143.
17. **Han C, Sun X, Liu L, Jiang H, Shen Y, Xu X, Li J, Zhang G, Huang J, Lin Z, Xiong N, Wang T.** Exosomes and their therapeutic potentials of stem cells. *Stem Cells Int* 2016: 7653489, 2016. doi:10.1155/2016/7653489.
18. **Hao L, Hao J, Fang W, Han C, Zhang K, Wang X.** Dual isotope simultaneous imaging to evaluate the effects of intracoronary bone marrow-derived mesenchymal stem cells on perfusion and metabolism in canines with acute myocardial infarction. *Biomed Rep* 3: 447–452, 2015. doi:10.3892/br.2015.474.
19. **Heldman AW, DiFede DL, Fishman JE, Zambrano JP, Trachtenberg BH, Karantalis V, Mushtaq M, Williams AR, Suncion VY, McNiece IK, Ghersin E, Soto V, Lopera G, Miki R, Willens H, Hendel R, Mitrani R, Pattany P, Feigenbaum G, Oskouei B, Byrnes J, Lowery MH, Sierra J, Pujol MV, Delgado C, Gonzalez PJ, Rodriguez JE, Bagno LL, Rouy D, Altman P, Foo CW, da Silva J, Anderson E, Schwarz R, Mendizabal A, Hare JM.** Transendocardial mesenchymal stem cells and mononuclear bone marrow cells for ischemic cardiomyop-

athy: the TAC-HFT randomized trial. *JAMA* 311: 62–73, 2014. doi:10.1001/jama.2013.282909.

20. **Hofmann M, Wollert KC, Meyer GP, Menke A, Arseniev L, Hertenstein B, Ganser A, Knapp WH, Drexler H.** Monitoring of bone marrow cell homing into the infarcted human myocardium. *Circulation* 111: 2198–2202, 2005. doi:10.1161/01.CIR.0000163546.27639.AA.
21. **Hou D, Youssef EA, Brinton TJ, Zhang P, Rogers P, Price ET, Yeung AC, Johnstone BH, Yock PG, March KL.** Radiolabeled cell distribution after intramyocardial, intracoronary, and interstitial retrograde coronary venous delivery: implications for current clinical trials. *Circulation* 112, *Suppl*: I150–I156, 2005. doi:10.1161/CIRCULATIONAHA.104.526749.
22. **Kang WJ, Kang HJ, Kim HS, Chung JK, Lee MC, Lee DS.** Tissue distribution of 18F-FDG-labeled peripheral hematopoietic stem cells after intracoronary administration in patients with myocardial infarction. *J Nucl Med* 47: 1295–1301, 2006. [Erratum in *J Nucl Med* 47:1399, 2006.]
23. **Karantalis V, DiFede DL, Gerstenblith G, Pham S, Symes J, Zambrano JP, Fishman J, Pattany P, McNiece I, Conte J, Schulman S, Wu K, Shah A, Breton E, Davis-Sproul J, Schwarz R, Feigenbaum G, Mushtaq M, Suncion VY, Lardo AC, Borrello I, Mendizabal A, Karas TZ, Byrnes J, Lowery M, Heldman AW, Hare JM.** Autologous mesenchymal stem cells produce concordant improvements in regional function, tissue perfusion, and fibrotic burden when administered to patients undergoing coronary artery bypass grafting: The Prospective Randomized Study of Mesenchymal Stem Cell Therapy in Patients Undergoing Cardiac Surgery (PROMETHEUS) trial. *Circ Res* 114: 1302–1310, 2014. doi:10.1161/CIRCRESAHA.114.303180.
24. **Klabunde RE.** *Cardiovascular Physiology Concepts*. Baltimore, MD: Lippincott Williams & Wilkins, 2011.
25. **Kossaify A.** Echocardiographic assessment of the right ventricle, from the conventional approach to speckle tracking and three-dimensional imaging, and insights into the "right way" to explore the forgotten chamber. *Clin Med Insights Cardiol* 9: 65–75, 2015. doi:10.4137/CMC.S27462.
26. **Kwon HM, Hur SM, Park KY, Kim CK, Kim YM, Kim HS, Shin HC, Won MH, Ha KS, Kwon YG, Lee DH, Kim YM.** Multiple paracrine factors secreted by mesenchymal stem cells contribute to angiogenesis. *Vascul Pharmacol* 63: 19–28, 2014. doi:10.1016/j.vph.2014.06.004.
27. **Lai RC, Arslan F, Lee MM, Sze NS, Choo A, Chen TS, Salto-Tellez M, Timmers L, Lee CN, El Oakley RM, Pasterkamp G, de Kleijn DP, Lim SK.** Exosome secreted by MSC reduces myocardial ischemia/reperfusion injury. *Stem Cell Res (Amst)* 4: 214–222, 2010. doi:10.1016/j.scr.2009.12.003.
28. **Lee PH, Tu CT, Hsiao CC, Tsai MS, Ho CM, Cheng NC, Hung TM, Shih DT.** Antifibrotic activity of human placental amnion membrane-derived CD34+ mesenchymal stem/progenitor cell transplantation in mice with thioacetamide induced liver injury. *Stem Cells Transl Med* 5: 1473–1484, 2016. doi:10.5966/sctm.2015-0343.
29. **Leeuwenburgh BP, Helbing WA, Steendijk P, Schoof PH, Baan J.** Biventricular systolic function in young lambs subject to chronic systemic right ventricular pressure overload. *Am J Physiol Heart Circ Physiol* 281: H2697–H2704, 2001. doi:10.1152/ajpheart.2001.281.6.H2697.
30. **Li L, Zhang Y, Li Y, Yu B, Xu Y, Zhao S, Guan Z.** Mesenchymal stem cell transplantation attenuates cardiac fibrosis associated with isoproterenol-induced global heart failure. *Transpl Int* 21: 1181–1189, 2008. doi:10.1111/j.1432-2277.2008.00742.x.
31. **Liu A, Philip J, Vinnakota KC, Van den Bergh F, Tabima DM, Hacker T, Beard DA, Chesler NC.** Estrogen maintains mitochondrial content and function in the right ventricle of rats with pulmonary hypertension. *Physiol Rep* 5: e13157, 2017. doi:10.14814/phy2.13157.
32. **Liu B, Lee BW, Nakanishi K, Villasante A, Williamson R, Metz J, Kim J, Kanai M, Bi L, Brown K, Di Paolo G, Homma S, Sims PA, Topkara VK, Vunjak-Novakovic G.** Cardiac recovery via extended cell-free delivery of extracellular vesicles secreted by cardiomyocytes derived from induced pluripotent stem cells. *Nat Biomed Eng* 2: 293–303, 2018. doi:10.1038/s41551-018-0229-7.
33. **Mangi AA, Noiseux N, Kong D, He H, Rezvani M, Ingwall JS, Dzau VJ.** Mesenchymal stem cells modified with Akt prevent remodeling and restore performance of infarcted hearts. *Nat Med* 9: 1195–1201, 2003. doi:10.1038/nm912.
34. **Maria ATJ, Toupet K, Maumus M, Fonteneau G, Le Quellec A, Jorgensen C, Guilpain P, Noël D.** Human adipose mesenchymal stem cells as potent anti-fibrosis therapy for systemic sclerosis. *J Autoimmun* 70: 31–39, 2016. doi:10.1016/j.jaut.2016.03.013.
35. **Mathiasen AB, Haack-Sørensen M, Jørgensen E, Kastrup J.** Autotransplantation of mesenchymal stromal cells from bone-marrow to heart in patients with severe stable coronary artery disease and refractory angina--final 3-year follow-up. *Int J Cardiol* 170: 246–251, 2013. doi:10.1016/j.ijcard.2013.10.079.
36. **Morrison TJ, Jackson MV, Cunningham EK, Kissenpfennig A, McAuley DF, O'Kane CM, Krasnodembskaya AD.** Mesenchymal stromal cells modulate macrophages in clinically relevant lung injury models by extracellular vesicle mitochondrial transfer. *Am J Respir Crit Care Med* 196: 1275–1286, 2017. doi:10.1164/rccm.201701-0170OC.
37. **Ooi CY, Wang Z, Tabima DM, Eickhoff JC, Chesler NC.** The role of collagen in extralobar pulmonary artery stiffening in response to hypoxia-induced pulmonary hypertension. *Am J Physiol Heart Circ Physiol* 299: H1823–H1831, 2010. doi:10.1152/ajpheart.00493.2009.
38. **Oommen S, Yamada S, Cantero Peral S, Campbell KA, Bruinsma ES, Terzic A, Nelson TJ.** Human umbilical cord blood-derived mononuclear cells improve murine ventricular function upon intramyocardial delivery in right ventricular chronic pressure overload. *Stem Cell Res Ther* 6: 50, 2015. doi:10.1186/s13287-015-0044-y.
39. **Rain S, Handoko ML, Trip P, Gan CT, Westerhof N, Stienen GJ, Paulus WJ, Ottenheijm CA, Marcus JT, Dorfmüller P, Guignabert C, Humbert M, Macdonald P, Dos Remedios C, Postmus PE, Saripalli C, Hidalgo CG, Granzier HL, Vonk-Noordegraaf A, van der Velden J, de Man FS.** Right ventricular diastolic impairment in patients with pulmonary arterial hypertension. *Circulation* 128: 2016–2025, 2013. doi:10.1161/CIRCULATIONAHA.113.001873.
40. **Schmuck EG, Koch JM, Centanni JM, Hacker TA, Braun RK, Eldridge M, Hei DJ, Hematti P, Raval AN.** Biodistribution and clearance of human mesenchymal stem cells by quantitative three-dimensional cryo-imaging after intravenous infusion in a rat lung injury model. *Stem Cells Transl Med* 5: 1668–1675, 2016. doi:10.5966/sctm.2015-0379.
41. **Schmuck EG, Koch JM, Hacker TA, Hatt CR, Tomkowiak MT, Vigen KK, Hendren N, Leitzke C, Zhao YQ, Li Z, Centanni JM, Hei DJ, Schwahn D, Kim J, Hematti P, Raval AN.** Intravenous followed by X-ray fused with MRI-guided transendocardial mesenchymal stem cell injection improves contractility reserve in a swine model of myocardial infarction. *J Cardiovasc Transl Res* 8: 438–448, 2015. doi:10.1007/s12265-015-9654-0.
42. **Schmuck EG, Mulligan JD, Ertel RL, Kouris NA, Ogle BM, Raval AN, Saupe KW.** Cardiac fibroblast-derived 3D extracellular matrix seeded with mesenchymal stem cells as a novel device to transfer cells to the ischemic myocardium. *Cardiovasc Eng Technol* 5: 119–131, 2014. doi:10.1007/s13239-013-0167-1.
43. **Spees JL, Whitney MJ, Sullivan DE, Lasky JA, Laboy M, Ylostalo J, Prockop DJ.** Bone marrow progenitor cells contribute to repair and remodeling of the lung and heart in a rat model of progressive pulmonary hypertension. *FASEB J* 22: 1226–1236, 2008. doi:10.1096/fj.07-8076com.
44. **Stenmark KR, Meyrick B, Galie N, Mooi WJ, McMurtry IF.** Animal models of pulmonary arterial hypertension: the hope for etiological discovery and pharmacological cure. *Am J Physiol Lung Cell Mol Physiol* 297: L1013–L1032, 2009. doi:10.1152/ajplung.00217.2009.
45. **Su LX, Guo YH, Guo N, Chang D, Xie LX, Liu CT.** The efficacy of MSC-HGF in treating pulmonary arterial hypertension (PAH) and connexin remodelling. *Cent Eur J Biol* 8: 240–251, 2013. doi:10.2478/s11535-013-0128-y.
46. **Suen CM, Zhai A, Lalu MM, Welsh C, Levac BM, Fergusson D, McIntyre L, Stewart DJ.** Efficacy and safety of regenerative cell therapy for pulmonary arterial hypertension in animal models: a preclinical systematic review protocol. *Syst Rev* 5: 89, 2016. doi:10.1186/s13643-016-0265-x.
47. **Sun CK, Lee FY, Sheu JJ, Yuen CM, Chua S, Chung SY, Chai HT, Chen YT, Kao YH, Chang LT, Yip HK.** Early combined treatment with cilostazol and bone marrow-derived endothelial progenitor cells markedly attenuates pulmonary arterial hypertension in rats. *J Pharmacol Exp Ther* 330: 718–726, 2009. doi:10.1124/jpet.109.154328.
48. **Tabima DM, Philip JL, Chesler NC.** Right ventricular-pulmonary vascular interactions. *Physiology (Bethesda)* 32: 346–356, 2017. doi:1152/physiol.00040.2016.
49. **Takemiya K, Kai H, Yasukawa H, Tahara N, Kato S, Imaizumi T.** Mesenchymal stem cell-based prostacyclin synthase gene therapy for pulmonary hypertension rats. *Basic Res Cardiol* 105: 409–417, 2010. doi:10.1007/s00395-009-0065-8.
50. **Tang J, Wang J, Zheng F, Kong X, Guo L, Yang J, Zhang L, Huang Y.** Combination of chemokine and angiogenic factor genes and mesenchymal stem cells could enhance angiogenesis and improve cardiac function after acute myocardial infarction in rats. *Mol Cell Biochem* 339: 107–118, 2010. doi:10.1007/s11010-009-0374-0.

51. **Umar S, de Visser YP, Steendijk P, Schutte CI, Laghmani H, Wagenaar GT, Bax WH, Mantikou E, Pijnappels DA, Atsma DE, Schalij MJ, van der Wall EE, van der Laarse A.** Allogenic stem cell therapy improves right ventricular function by improving lung pathology in rats with pulmonary hypertension. *Am J Physiol Heart Circ Physiol* 297: H1606–H1616, 2009. doi:10.1152/ajpheart.00590.2009.
52. **Umar S, Steendijk P, Ypey DL, Atsma DE, van der Wall EE, Schalij MJ, van der Laarse A.** Novel approaches to treat experimental pulmonary arterial hypertension: a review. *J Biomed Biotechnol* 2010: 702836, 2010. doi:10.1155/2010/702836.
53. **Van den Bergh A, Flameng W, Herijgers P.** Parameters of ventricular contractility in mice: influence of load and sensitivity to changes in inotropic state. *Pflugers Arch* 455: 987–994, 2008. doi:10.1007/s00424-007-0362-8.
54. **van der Laarse A, Cobbaert CM, Umar S.** Stem and progenitor cell therapy for pulmonary arterial hypertension: effects on the right ventricle (2013 Grover Conference Series). *Pulm Circ* 5: 73–80, 2015. doi:10.1086/679701.
55. **Voelkel NF, Gomez-Arroyo J, Abbate A, Bogaard HJ.** Mechanisms of right heart failure—A work in progress and a plea for failure prevention. *Pulm Circ* 3: 137–143, 2013. doi:10.4103/2045-8932.109957.
56. **Voelkel NF, Gomez-Arroyo J, Abbate A, Bogaard HJ, Nicolls MR.** Pathobiology of pulmonary arterial hypertension and right ventricular failure. *Eur Respir J* 40: 1555–1565, 2012. doi:10.1183/09031936.00046612.
57. **Voelkel NF, Quaife RA, Leinwand LA, Barst RJ, McGoon MD, Meldrum DR, Dupuis J, Long CS, Rubin LJ, Smart FW, Suzuki YJ, Gladwin M, Denholm EM, Gail DB; National Heart, Lung, and Blood Institute Working Group on Cellular and Molecular Mechanisms of Right Heart Failure.** Right ventricular function and failure: report of a National Heart, Lung, and Blood Institute working group on cellular and molecular mechanisms of right heart failure. *Circulation* 114: 1883–1891, 2006. doi:10.1161/CIRCULATIONAHA.106.632208.
58. **Vonk-Noordegraaf A, Haddad F, Chin KM, Forfia PR, Kawut SM, Lumens J, Naeije R, Newman J, Oudiz RJ, Provencher S, Torbicki A, Voelkel NF, Hassoun PM.** Right heart adaptation to pulmonary arterial hypertension: physiology and pathobiology. *J Am Coll Cardiol* 62, *Suppl*: D22–D33, 2013. doi:10.1016/j.jacc.2013.10.027.
59. **Walker LA, Buttrick PM.** The right ventricle: biologic insights and response to disease: updated. *Curr Cardiol Rev* 9: 73–81, 2013.
60. **Wang Z, Patel JR, Schreier DA, Hacker TA, Moss RL, Chesler NC.** Organ-level right ventricular dysfunction with preserved Frank-Starling mechanism in a mouse model of pulmonary arterial hypertension. *J Appl Physiol (1985)* 124: 1244–1253, 2018. doi:10.1152/japplphysiol.00725.2017.
61. **Wang Z, Schreier DA, Hacker TA, Chesler NC.** Progressive right ventricular functional and structural changes in a mouse model of pulmonary arterial hypertension. *Physiol Rep* 1: e00184, 2013. doi:10.1002/phy2.184.
62. **Wehman B, Sharma S, Pietris N, Mishra R, Siddiqui OT, Bigham G, Li T, Aiello E, Murthi S, Pittenger M, Griffith B, Kaushal S.** Mesenchymal stem cells preserve neonatal right ventricular function in a porcine model of pressure overload. *Am J Physiol Heart Circ Physiol* 310: H1816–H1826, 2016. doi:10.1152/ajpheart.00955.2015.
63. **Williams AR, Trachtenberg B, Velazquez DL, McNiece I, Altman P, Rouy D, Mendizabal AM, Pattany PM, Lopera GA, Fishman J, Zambrano JP, Heldman AW, Hare JM.** Intramyocardial stem cell injection in patients with ischemic cardiomyopathy: functional recovery and reverse remodeling. *Circ Res* 108: 792–796, 2011. doi:10.1161/CIRCRESAHA.111.242610.
64. **Xu J, Nagata K, Obata K, Ichihara S, Izawa H, Noda A, Nagasaka T, Iwase M, Naoe T, Murohara T, Yokota M.** Nicorandil promotes myocardial capillary and arteriolar growth in the failing heart of Dahl salt-sensitive hypertensive rats. *Hypertension* 46: 719–724, 2005. doi:10.1161/01.HYP.0000185189.46698.15.
65. **Yen CH, Tsai TH, Leu S, Chen YL, Chang LT, Chai HT, Chung SY, Chua S, Tsai CY, Chang HW, Ko SF, Sun CK, Yip HK.** Sildenafil improves long-term effect of endothelial progenitor cell-based treatment for monocrotaline-induced rat pulmonary arterial hypertension. *Cytotherapy* 15: 209–223, 2013. doi:10.1016/j.jcyt.2012.09.002.
66. **Yerebakan C, Sandica E, Prietz S, Klopsch C, Ugurlucan M, Kaminski A, Abdija S, Lorenzen B, Boltze J, Nitzsche B, Egger D, Barten M, Furlani D, Ma N, Vollmar B, Liebold A, Steinhoff G.** Autologous umbilical cord blood mononuclear cell transplantation preserves right ventricular function in a novel model of chronic right ventricular volume overload. *Cell Transplant* 18: 855–868, 2009. doi:10.3727/096368909X471170.
67. **Zhang J, Zhu W, Radisic M, Vunjak-Novakovic G.** Can we engineer a human cardiac patch for therapy? *Circ Res* 123: 244–265, 2018. doi:10.1161/CIRCRESAHA.118.311213.
68. **Zuo HJ, Liu ZX, Liu XC, Yang J, Liu T, Wen S, Wang DW, Zhang X.** Assessment of myocardial blood perfusion improved by CD151 in a pig myocardial infarction model. *Acta Pharmacol Sin* 30: 70–77, 2009. doi:10.1038/aps.2008.10.